Signature of pseudogap formation in the density of states of underdoped cuprates

A. J. H. Borne,[1,2,3] J. P. Carbotte,[4,5] and E. J. Nicol[1,2,*]
[1]*Department of Physics, University of Guelph, Guelph, Ontario, Canada N1G 2W1*
[2]*Guelph-Waterloo Physics Institute, University of Guelph, Guelph, Ontario, Canada N1G 2W1*
[3]*PHELMA Grenoble INP, MINATEC, 3 Parvis Louis Néel, BP 275, 38016 Grenoble Cedex 1, France*
[4]*Department of Physics and Astronomy, McMaster University, Hamilton, Ontario, Canada L8S 4M1*
[5]*The Canadian Institute for Advanced Research, Toronto, Ontario, Canada M5G 1Z8*
(Received 9 June 2010; published 27 July 2010)

The resonating valence bond spin liquid model for the underdoped cuprates has as an essential element, the emergence of a pseudogap. This energy scale introduces asymmetry in the quasiparticle density of states because it is associated with the antiferromagnetic Brillouin zone. By contrast, superconductivity develops on the Fermi surface and this largely restores the particle-hole symmetry for energies below the superconducting energy-gap scale. In the highly underdoped regime, these two scales can be separately identified in the density of states and also partial density of states for each fixed angle in the Brillouin zone. From the total density of states, we find that the pseudogap energy scale manifests itself differently as a function of doping for positive and negative biases. Furthermore, we find evidence from recent scanning tunneling spectroscopy data for asymmetry in the positive and negative biases of the extracted $\Delta(\theta)$ which is in qualitative agreement with this model. Likewise, the slope of the linear low-energy density of states is nearly constant in the underdoped regime while it increases significantly with overdoping in agreement with the data.

DOI: 10.1103/PhysRevB.82.024521 PACS number(s): 74.72.−h, 74.20.Mn, 74.55.+v

I. INTRODUCTION

BCS theory modified to account for *d*-wave symmetry of the superconducting order parameter has provided a solid basis for a first understanding of the properties of the cuprates around optimum and in the overdoped regime. However, the underdoped region of the phase diagram provides challenges to such a simple approach. These systems present many features that have been considered anomalous and are not part of simple BCS theory. While the subject remains controversial and very different ideas have been put forward to understand these anomalies, a recently developed model by Yang, Rice, and Zhang (YRZ) (Ref. 1) which is based on a spin liquid resonating valence bond approach, has had considerable success in this direction. It is very different from the preformed pair model[2] where a superconducting gap forms at a high temperature, the pseudogap temperature T^*, and the superconductivity appears only at a lower temperature T_c as a result of the onset of phase coherence. The YRZ model has a central element, an energy scale, the pseudogap Δ_{pg}, which is responsible for changes in the electronic structure of the normal state above T_c. The pseudogap is distinct from the superconducting gap Δ_{sc} and the superconducting state is conceived as forming from this normal pseudogap phase which is quite different from an ordinary Fermi-liquid (FL) state. In the YRZ model, the large Fermi surface (FS) of FL theory (FLT) reconstructs into hole and electron pockets as a result of the growth in pseudogap at doping levels x, in the underdoped region of the cuprate phase diagram, with $x<x_c$, where x_c is the doping associated with a quantum critical point (QCP).

The model is related but different from other competing order proposals such as *d*-density wave formation[3,4] and has the desirable property that, in its final form, it remains simple and has been successfully applied to the calculation of many superconducting properties.[5–12] Besides a self-energy which accounts for the formation of a pseudogap on the antiferromagnetic Brillouin-zone (AFBZ) boundary, the model has Gutzwiller factors modifying the underlying band-structure parameters. These narrow the bands as correlation effects become more important. Also, a Gutzwiller factor accounts for the loss of coherence which greatly reduces the weight of the remaining quasiparticle peak as the incoherent background increases. These elements account for the approach to the Mott insulating state which is best understood near half filling in a localized picture of electron dynamics. The hopping from one site to another is blocked by a large Hubbard U which describes the energy cost for double occupancy. The pseudogap and AFBZ then play a role similar to a band gap at the Brillouin zone in ordinary band theory but with essential differences. For example, in YRZ, the bands are not filled rigidly with decreasing doping but instead undergo profound changes as the pseudogap increases.

Among the properties already calculated and compared with experiment are Raman,[5,6] specific heat,[7] optical properties,[8] aspects of angular-resolved photoemission spectroscopy, and scanning tunneling spectroscopy (STS) (Ref. 9) including the checkerboard pattern,[10] Andreev tunneling,[11] and also the penetration depth.[12] Each of these properties show behaviors which cannot be understood in *d*-wave BCS nor in it extensions to include inelastic scattering,[13–20] anisotropy,[21–25] or strong-coupling effects rooted in Eliashberg theory.[24–26] Among the previously considered anomalous properties that are now understood are the two distinct gap scales seen in Raman spectra. The B_{2g} peak decreases with decreasing doping while the B_{1g} scale increases instead.[5,6] The normalized jump in the specific heat drops rather precipitously as x decreases toward the bottom of the superconducting dome.[7] New structures are seen in the optical self-energy and the two energy scales found in the partial optical sum as a function of energy are understood.[8] The

rapid drop in the superfluid density at zero temperature with decreasing x while the slope of the low temperature linear in T law is relatively only weakly changed is also shown.[12] Encouraged by these successes, here we consider the quasiparticle density of states (DOS).

In Sec. II, we present the formalism of YRZ (Ref. 1) for the electron spectral density in the underdoped regime. It includes pseudogap formation below a QCP at a doping of $x=x_c=0.2$. We describe how this energy scale modifies the electronic structure from the usual large Fermi surface of FLT to Luttinger pockets. There are two energy branches in the theory $E_k^{\pm}$, with E_k^- giving a hole pocket and E_k^+ an electron pocket, the latter only in a restricted doping range just below x_c. For very underdoped samples, only the hole pocket remains. In Sec. III, we present our results for the quasiparticle DOS with and without superconductivity and also breakup the results into their partial contributions from each of the two energy branches separately. We discuss how the pseudogap alone introduces an asymmetry between positive and negative biases in the DOS $N(\omega)$ and how superconductivity overrides this effect and so restores particle-hole symmetry at small energies of order the superconducting gap energy Δ_{sc}^0. At higher energy, asymmetry remains. We also show that modifications in the DOS introduced by superconductivity which are confined to a range of a few times Δ_{sc}^0 in the case of a Fermi liquid extend instead over the range of the pseudogap energy scale in YRZ. In Sec. IV, we consider decomposing the total quasiparticle DOS into partial contributions from fixed angle θ measured from (π,π) in the upper right quadrant of the Brillouin zone. These partial distributions can display several structures. Nevertheless, upon examination we are able to define for each direction θ an energy gap associated with a specific peak in the partial DOS. This peak which is taken mainly, but not always, to correspond to the smallest energy closest to $\omega=0$, is sometimes the superconducting gap peak but can also be a pseudogap peak. The energies extracted in this way show considerable anisotropy between positive and negative biases which is a fundamental characteristic of the model used here. We find evidence in experiment for this anisotropy and provide a comparison with STS data. In Sec. V, we discuss the limit of low bias where the DOS is linear in ω. We recover the FL result with an extra Gutzwiller factor reflecting the strong correlations in the system. Section VI contains a summary and conclusions.

II. FORMALISM

The spectral function for the coherent part of the electronic propagator in the model of Yang, Rice, and Zhang[1] takes the form

$$A(\boldsymbol{k},\omega)=\sum_{\alpha=\pm} g_t(x)W_{\boldsymbol{k}}^{\alpha}[(u_{\boldsymbol{k}}^{\alpha})^2\delta(\omega-E_S^{\alpha})+(v_{\boldsymbol{k}}^{\alpha})^2\delta(\omega+E_S^{\alpha})], \tag{1}$$

where $E_S^{\alpha}=\sqrt{(E_{\boldsymbol{k}}^{\alpha})^2+\Delta_{sc}^2(\boldsymbol{k})}$ are the quasiparticle energies in the superconducting state with $(u_{\boldsymbol{k}}^{\alpha})^2$ and $(v_{\boldsymbol{k}}^{\alpha})^2$ the corresponding Bogoliubov amplitudes. In Eq. (1), the $W_{\boldsymbol{k}}^{\alpha}$ ($\alpha=\pm$) are the weighting factors of the YRZ theory which involve the input pseudogap $\Delta_{pg}(\boldsymbol{k})$ and do not change in the superconducting state. They depend on the electronic band-structure energies $\xi_{\boldsymbol{k}}$ as well as the umklapp surface energy $\xi_{\boldsymbol{k}}^0$. Specifically,

$$W_{\boldsymbol{k}}^{\pm}=\frac{1}{2}\left(1\pm\frac{\tilde{\xi}_{\boldsymbol{k}}}{E_{\boldsymbol{k}}}\right) \tag{2}$$

with $\tilde{\xi}_{\boldsymbol{k}}=(\xi_{\boldsymbol{k}}+\xi_{\boldsymbol{k}}^0)/2$ and $E_{\boldsymbol{k}}=\sqrt{\tilde{\xi}_{\boldsymbol{k}}^2+\Delta_{pg}^2(\boldsymbol{k})}$. In the nonsuperconducting state, the energies have two branches $E_{\boldsymbol{k}}^{\pm}=(\xi_{\boldsymbol{k}}-\xi_{\boldsymbol{k}}^0)/2\pm E_{\boldsymbol{k}}$ and in the superconducting state, the Bogoliubov weights are given in terms of these by

$$(u_{\boldsymbol{k}}^{\alpha})^2=\frac{1}{2}\left(1+\frac{E_{\boldsymbol{k}}^{\alpha}}{E_S^{\alpha}}\right), \tag{3}$$

$$(v_{\boldsymbol{k}}^{\alpha})^2=\frac{1}{2}\left(1-\frac{E_{\boldsymbol{k}}^{\alpha}}{E_S^{\alpha}}\right). \tag{4}$$

In the YRZ paper, the band energies, taken to include up to third-nearest-neighbor hopping, are $\xi_{\boldsymbol{k}}=-2t(x)(\cos k_x a+\cos k_y a)-4t'(x)\cos k_x a\cos k_y a-2t''(x)(\cos 2k_x a+\cos 2k_y a)-\mu_p$, where μ_p is the chemical potential adjusted to obtain the correct number of electrons, through a procedure based on Luttinger's theorem. The umklapp surface energy is where $\xi_{\boldsymbol{k}}^0=-2t(x)(\cos k_x a+\cos k_y a)$ equals zero. Here a is the two-dimensional CuO_2 plane lattice parameter. The form of the hopping coefficients $t(x)$, $t'(x)$, and $t''(x)$ are fixed in the YRZ model[1] and will not be changed in this work except to note that t_0 enters as a proportionality factor in these hoppings and consequently all our results scale by t_0 and so this parameter can be varied at will. The Gutzwiller factor $g_t(x)$ which appears as a simple multiplicative factor in Eq. (1) provides a measure of the remaining quasiparticle strength in the coherent part of the Green's function. Along with a second Gutzwiller factor $g_s(x)$, it also enters the band structure, through $t(x)$, $t'(x)$, and $t''(x)$, which provides narrower bands as the doping x is reduced toward the Mott insulating state at half filling. Specifically, $g_t(x)=2x/(1+x)$ and $g_s(x)=4/(1+x)^2$.

For the input superconducting gap, YRZ take

$$\Delta_{sc}(\boldsymbol{k})=\frac{\Delta_{sc}^0(x)}{2}(\cos k_x a-\cos k_y a) \tag{5}$$

and likewise the same form for $\Delta_{pg}(\boldsymbol{k})$ with the gap amplitude $\Delta_{pg}^0(x)$ replacing the superconducting gap amplitude in Eq. (5). Both have the simplest d-wave form characterized by the lowest harmonic having the required symmetry. The amplitudes in Eq. (5) and equivalently for the pseudogap are

$$\Delta_{sc}^0(x)=0.14t_0[1-82.6(x-0.2)^2], \tag{6}$$

$$\Delta_{pg}^0(x)=3t_0(0.2-x), \tag{7}$$

where both are taken to be proportional to t_0 and the QCP at which the pseudogap gap becomes nonzero is $x_c=0.2$, where the superconducting gap is also taken to have its optimum value. This last condition can easily be relaxed to have the

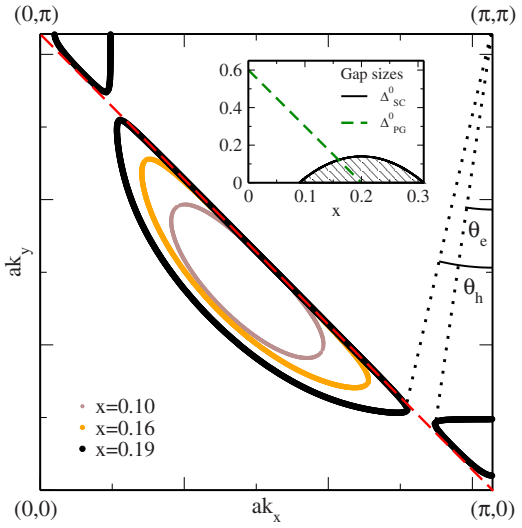

FIG. 1. (Color online) The reconstructed Fermi-surface contours for three values of doping: $x=0.10$ (brown), 0.16 (yellow), and 0.19 (black), shown in the upper right quadrant of the square Brillouin zone. The black contours have both hole and electron Luttinger pockets (located around the nodal and antinodal directions, respectively). The angles measured from (π,π) which define the end of these pockets are θ_h and θ_e, respectively. The inset shows the superconducting dome and pseudogap line as a function of doping defined via $\Delta^0_{\rm sc}$ and $\Delta^0_{\rm pg}$ in the YRZ model.

maximum gap at 0.16 instead (as in experiment).

In Fig. 1, we show how the Fermi-surface contours evolve with doping. At the QCP ($x=0.2$) there is no pseudogap in the YRZ model and the Fermi surface is the usual large open surface of FLT. As x is lowered into the underdoped regime, the Fermi surface reconstructs and Luttinger contours of zero energy emerge. They correspond to either $E^-_{\boldsymbol{k}}=0$ or $E^+_{\boldsymbol{k}}=0$. The solutions for the first case give the hole pockets centered on the nodal direction and these exist for $\theta=\pi/4$ to θ_h as indicated in the figure. For the case of $x=0.19$ but not for the other values of doping shown, there is an additional electron pocket ($E^+_{\boldsymbol{k}}=0$) located in the region between the AFBZ boundary (dashed red line) and the Brillouin zone which extends from $\theta=\theta_e$ to $\theta=0$, where θ is an angle measured from the origin (π,π) in the right-hand upper quadrant of the Brillouin zone as shown. In both cases for hole and electron contours, solutions to the equation $E^{\pm}_{\boldsymbol{k}}=0$ when they exist (for a given angle θ) always come in pairs. For some angles however, there is no solution at all. When two solutions exist, the backside of the Luttinger pocket closest to the AFBZ boundary (red dashed line) has only a small weight $W^{\pm}_{\boldsymbol{k}}$ as compared with the front part which is orientated toward the center of the Brillouin zone for the hole pocket and oppositely for the electron pocket. Both of these have weight of order one and this is the piece of the FS which corresponds to the FL when the pseudogap goes to zero. The backsides instead go into the AFBZ boundary and have weight exactly equal to zero in this same limit. As seen in the figure, when x moves toward the Mott insulating state, the Luttinger hole pocket becomes increasingly short with θ_h moving toward the nodal direction and this is the agency whereby the metallicity of the material is increasingly reduced. The number

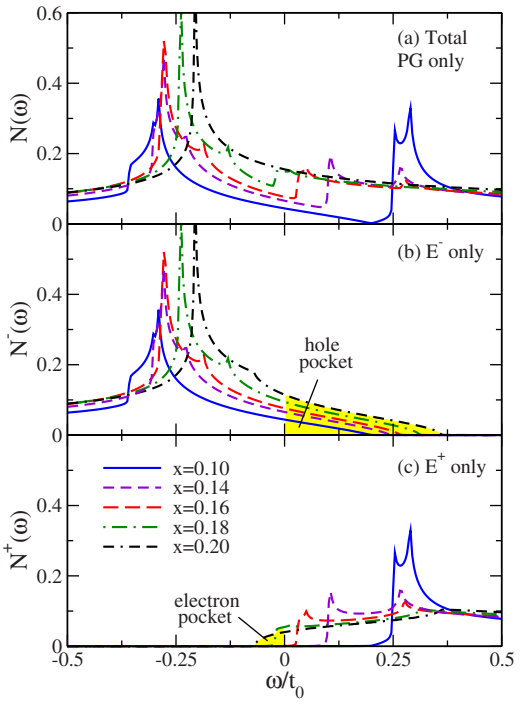

FIG. 2. (Color online) Density of quasiparticle states $N(\omega)$ in the pseudogap state as a function of ω in units of t_0. (a) shows the total DOS, and (b) and (c) give the partial results from the $E^-_{\boldsymbol{k}}$ and $E^+_{\boldsymbol{k}}$ branches separately. The shaded yellow region in (b) and (c) identifies the contribution of hole and electron pockets, respectively.

of states with significant weighting and zero excitation energy is reduced. The approach to half filling has a progressively stronger detrimental effect on the dynamics of the charge carriers due to the increased magnitude of the pseudogap which has opened on the AFBZ boundary. An important point to note is that the branch $E^-_{\boldsymbol{k}}$ corresponds to negative energy except for momenta forming the hole pocket while $E^+_{\boldsymbol{k}}$ corresponds to positive energies except for momenta inside the electron pocket.

III. RESULTS FOR THE DENSITY OF QUASIPARTICLE STATES

In Fig. 2, we show the quasiparticle DOS corresponding to each band separately in frames (b) and (c), $N^-(\omega)$ and $N^+(\omega)$, respectively, with the total $N(\omega)=N^-(\omega)+N^+(\omega)$ given in frame (a). Here, $N^{\pm}(\omega)$ is the sum over the Brillouin zone of $g_t(x)W^{\pm}_{\boldsymbol{k}}\delta(\omega-E^{\pm}_{\boldsymbol{k}})$. The double-dashed-dotted black curve for $N^-(\omega)$ gives results for $x=0.2$ which has no pseudogap and corresponds to the usual Fermi-liquid band structure. If to this we add the contribution from $N^+(\omega)$ in frame (c), we obtain the usual FL result shown as the double-dashed-dotted black curve for the total DOS in (a). It extends over an energy range of order several t_0 and has a van Hove (VH) singularity at an energy slightly above $-0.25t_0$. The energy scale on which the DOS can vary significantly, however, is set by the bandwidth except for the rapid variation around the van Hove singularity but we will not emphasize this aspect. Returning to the frames (b) and (c) of Fig. 2, the

areas shaded in yellow for emphasis correspond, respectively, to the contributions for hole and electron Luttinger pockets. Note, in particular, that the shaded region for $N^+(\omega)$ exists only for dopings near optimum which is the only regime for which electron pockets appear. As the doping is decreased toward the Mott transition, a gap forms in this band above $\omega=0$ and there is a sharp rise in DOS at some finite frequency above which states are seen to pile up before $N^+(\omega)$ returns to a value closer to its no pseudogap value. The energy associated with the sharp rise in $N^+(\omega)$ can be identified as an effective pseudogap value, it is different from the input pseudogap although it is of the same order in magnitude. In fact, the net effect of the input pseudogap can be a depression which can even fall at negative energies as can be seen clearly in the composite curve shown in the top frame (a) for $x=0.18$. The DOS coming from the negative branch $E_{\boldsymbol{k}}^-$ also shows a clear effect of pseudogap formation when compared with the double-dashed-dotted black curve. We see a shift of the main van Hove singularity (present in the FL case) to lower energies, followed by a depression at higher energies beyond a second relatively smaller van Hove structure. The position in energy of this second structure can be taken as a second measure of an effective pseudogap.

In the upper curve for the total DOS, the two scales identified as due to the pseudogap combine to give a dip in the FL DOS which initially, for small pseudogap, is confined to the region of negative energies and is not at the Fermi surface as is often assumed in phenomenological models of the pseudogap. This dip grows with decreasing x both in range over which it extends and in depth. For small x it ranges over a large energy region and becomes a dominant feature in the DOS which is also greatly reduced around the Fermi energy $\omega=0$. It is important to emphasize that the pseudogap can introduce significant anisotropy between positive and negative values of ω beyond the relatively mild particle-hole asymmetry of the starting FL band structure. This is an essential element of the YRZ model which would not arise if the pseudogap opened on the Fermi surface rather than on the AFBZ boundary. In this regard Fig. 3 is particularly relevant. It shows our results when, in addition to a pseudogap, we include a superconducting gap. Because this second gap opens on the Fermi surface it produces a new total DOS which is much more particle-hole symmetric about $\omega=0$ than was the underlying pseudogap-only DOS, for energies of order of the superconducting gap. Before emphasizing this important point further, we note that the opening of the superconducting gap has pushed some spectral weight in $N^+(\omega)$ to lower negative energies due to the Bogoliubov coherence factors characteristic of Cooper pairing. The peak at the gap at negative energies is quite significant in magnitude.

In Fig. 4, we compare results of calculations for $x=0.16$ when only a superconducting gap is present (solid red curve) and when in addition there is also a pseudogap (dashed blue curve). For the solid curve, the superconducting coherence peaks fall symmetrically at $\omega=\pm 0.11$ even though the underlying FL DOS has a van Hove singularity which appears only at negative bias. There is as well a second peak at $\omega=\pm 0.23$ which is the normal-state van Hove singularity slightly shifted by the superconductivity and now appearing at both positive and negative biases although its positive bias

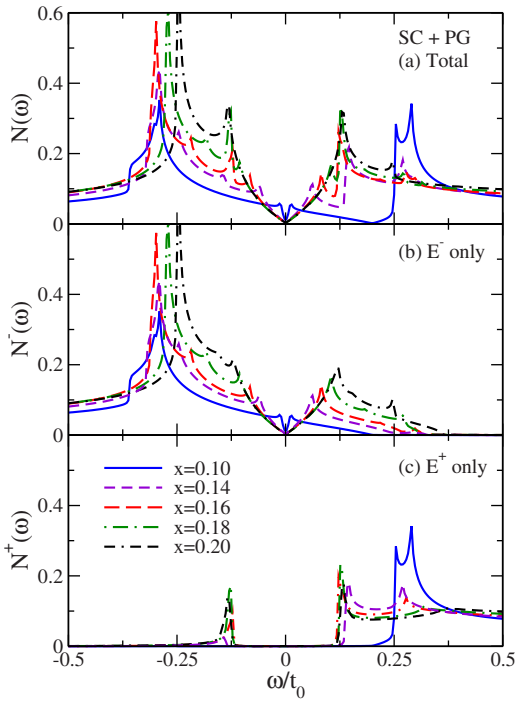

FIG. 3. (Color online) Density of quasiparticle states $N(\omega)$ when both the superconducting and pseudogap are included, as a function of ω in units of t_0. Similar to Fig. 2, (a) shows the total DOS, and (b) and (c) give the partial results for $E_{k,S}^-$ and $E_{k,S}^+$ branches, respectively.

image is greatly suppressed in amplitude. More surprisingly for the pseudogap case, the symmetry between positive and negative ω remains in that there are peaks at $\omega=\pm 0.08$ and ± 0.12 as well as at $\omega=\pm 0.22$ and even at $\omega=\pm 0.30$. But of course the magnitude of each peak in a given pair can be very different. The asymmetry prominent in the nonsuperconducting state has been greatly suppressed by the onset of the superconducting gap. Finally note that at low bias, the dashed blue curve and solid red curve agree very well and the introduction of the pseudogap has had no effect on this region of energy. We will return to this issue later in Sec. V.

Having just emphasized the restoration of particle-hole symmetry through superconductivity, we explore next the

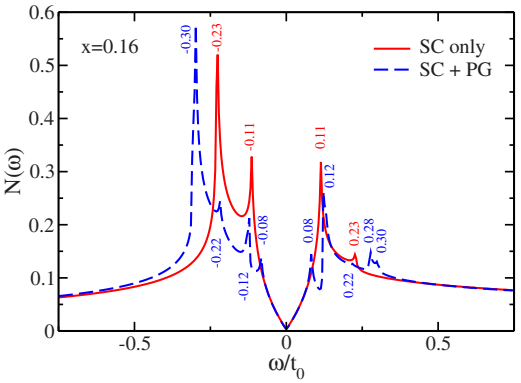

FIG. 4. (Color online) Comparison of the total DOS $N(\omega)$ versus ω in units of t_0 for doping $x=0.16$. Superconductivity is included in both curves. The dashed blue curve includes the pseudogap.

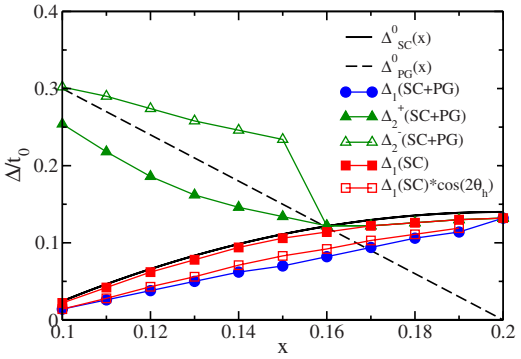

FIG. 5. (Color online) Energy scales extracted from total quasiparticle density of states as a function of doping x. Black solid and dashed curves are for comparison and are the amplitudes of the input gap $\Delta^0_{sc}(x)$ and $\Delta^0_{pg}(x)$, respectively. The solid red squares are taken from the superconducting coherence peak position when the pseudogap is set to zero and the open red squares are $\cos(2\theta_h)$ times the value of the solid red squares. With the pseudogap on, the positive and negative biases give different energy scales associated with resolvable peaks in $N(\omega)$. The green triangles are the superconducting gap peaks at larger dopings $x \gtrsim 0.16$ and the solid blue dots are secondary superconducting gap peaks associated with the end of the Luttinger hole pocket. For $x \lesssim 0.16$, the filled and open triangles are the pseudogap peaks for positive and negative biases, respectively.

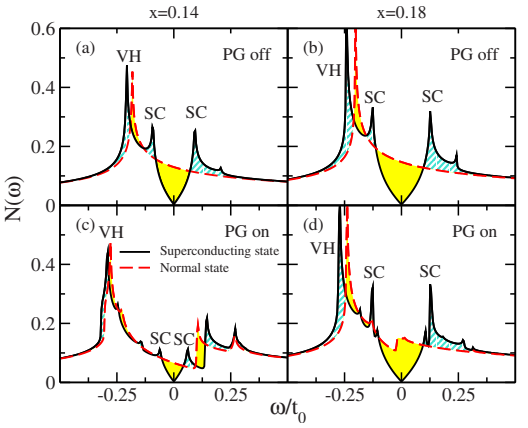

FIG. 6. (Color online) The quasiparticle DOS $N(\omega)$ with the pseudogap [(a) and (b)] off and [(c) and (d)] on for two doping values $x=0.14$ (left frames) and 0.18 (right frames). Comparison is made between the normal state (red dashed curve) which has no superconductivity and the case with superconductivity (black solid curve). The yellow solid shading and the blue hatched shading help to see the conservation of states.

asymmetry which nevertheless remains in the quasiparticle DOS and which can be traced to the pseudogap. In Fig. 5, the solid black curve gives the input superconducting gap amplitude $\Delta^0_{sc}(x)$ as a function of doping from $x=0.2$ (the QCP) to $x=0.1$, close to the end of the superconducting dome for the parameters used by YRZ. The solid red squares were obtained in the FL calculations based on the underlying large Fermi surfaces assuming $\Delta^0_{pg}(x)=0$ at all dopings. These points are taken from the energy of the superconducting coherence peaks in these calculations and fall slightly below the input values for $\Delta^0_{sc}(x)$. This is expected since the peak in the DOS is representative of the extremal value of the superconducting gap on the Fermi surface rather than in the Brillouin zone and these are slightly different. When both the superconductivity and the pseudogap are present, the peak structure in $N(\omega)$ becomes more complex. The lowest energy peaks in the top frame of Fig. 3 are associated with the superconducting gap. Starting with the most underdoped case first, solid blue curve for $x=0.1$, we see suppressed coherence peaks as compared to their magnitude in the optimum case $x=0.2$ (black double-dashed-dotted curve). Also, the energy at which they occur is considerably less than the value of the input gap amplitude. We plot these in Fig. 5 as the solid blue circles and see that they trace a dome but in all cases fall considerably below the input gap amplitude curve (solid black line). These points correspond to the gap at the edge of the Luttinger hole pocket and are therefore considerably smaller in energy than $\Delta^0_{sc}(x)$. In fact, we show as open red squares, the product of the solid red squares times $\cos(2\theta_h)$ (see Fig. 1) and these agree very well with the solid blue circles. In all cases, the solid and open green triangles for positive and negative biases, respectively, are the energies associated with the second significant or resolvable peak closest to $\omega=0$. These points fall very close to the superconducting coherence peak energies of the corresponding FL for $x \gtrsim 0.16$ (the triangles are underneath the solid squares for $x \gtrsim 0.17$ in Fig. 5) and are the same for positive and negative biases ω, i.e., we have particle-hole symmetry in this case. We also conclude that for this range of doping, these peaks are the primary superconducting coherence peaks even when the pseudogap is present and further they remain largely unmodified from the FL $\Delta^0_{pg}(x)=0$ case. In this sense for these cases, the superconducting gap has largely overridden the effect of the pseudogap. This all changes for $x \lesssim 0.16$. In those cases, the energy of the second peak is quite different for positive and negative biases and these pseudogap peaks exhibit a great deal of anisotropy. This second energy scale is also seen in Raman scattering[27] where the nodal B_{2g} geometry probes the superconducting gap scale and the B_{1g} antinodal geometry, the pseudogap. As we have seen here, when optimum doping is approached, the two scales are found to merge into a single superconducting gap scale. What is different, however, is that the DOS peak structure can be exploited to get information on the asymmetric effect of the pseudogap between positive and negative energies. Our results in Fig. 5 show that this can be considerable and that the effect sets in quite abruptly around $x=0.16$ when only the hole Luttinger pocket remains.

Figure 6 shows results for the DOS at two dopings $x=0.14$ (left frames) and $x=0.18$ (right frames). The top frames compare results for normal (red dashed curve) and superconducting state (black solid curve). The yellow solid shading and blue hatched regions help one to see that our calculations conserve the number of states between the normal and superconducting cases as they must. What is clear from the figure and what we wish to emphasize here is that when there is no pseudogap, the states lost below the superconducting gap are largely recovered just above the coherence peak except for a small shift in the VH singularity which introduces a slight complication that would not be present in models with a constant DOS. When the pseudogap

is included there is further readjustment of spectral weight introduced by the transition to the superconducting state. The energy range over which there remains significant changes is now set by the pseudogap scale. Here we are not emphasizing the slight complication brought about by the existence of a van Hove singularity in the underlying band structure chosen in the YRZ model.

IV. DECOMPOSITION OF DOS IN ANGLES IN THE BRILLOUIN ZONE

We turn next to the decomposition of the total DOS into partial contributions coming from different angular slices in the Brillouin zone. Such a decomposition has been considered by Pushp *et al.*[28] in relation to their experimental STS results. They effectively decompose the total $N(\omega)$ by writing

$$N(\omega) \equiv \int_0^{2\pi} \frac{d\theta}{2\pi} N(\omega,\theta), \tag{8}$$

where for $N(\omega,\theta)$, they take the explicit analytic functional form

$$N(\omega,\theta) = \mathrm{Re}\left\{ \frac{\omega - i\Gamma}{\sqrt{(\omega - i\Gamma)^2 - \Delta(\theta)^2}} \right\} W(\theta), \tag{9}$$

where Γ is a smearing parameter to be varied to get a best fit of the data along with the value of the gap $\Delta(\theta)$ and weighting factor $W(\theta)$. In this way, a gap scale $\Delta(\theta)$ can be obtained as a function of θ. Inspired by the above, we decompose the full density of states

$$N(\omega) = \sum_{\boldsymbol{k}} A(\boldsymbol{k},\omega), \tag{10}$$

where $A(\boldsymbol{k},\omega)$ is given in Eq. (1), into an integration over the magnitude of momentum k for fixed angle θ in the Brillouin zone. This gives $N(\omega,\theta)$ directly and results are presented in Fig. 7. Frame (a) is for doping $x=0.12$ and (b) for $x=0.18$. Twenty six values of θ are shown between 45° and 0° as measured from the (π,π) point of the Brillouin zone (see Fig. 1). The nodal direction (top curves) show small coherence peaks due to superconductivity which are centered about $\omega=0$ and are particle-hole symmetric. At higher positive energies, we see that there are two more pseudogap peaks while at negative bias, a van Hove singularity is seen.

In Fig. 8, we show results for $E_{\boldsymbol{k}}^{+}$ and $E_{\boldsymbol{k}}^{-}$ as a function of absolute value of momentum $|\boldsymbol{k}|=k$ measured from (π,π) for several values of angle θ measured similarly as the angles shown in Fig. 1 and used for Fig. 7. Doping was set at $x=0.14$. The pseudogap Dirac point falls at $\theta=\pi/4$ and $k=2.45$ in units of $1/a$ (solid black curves) and this corresponds to $E_{\boldsymbol{k}}^{+}=E_{\boldsymbol{k}}^{-}=0.24$ in units of the unrenormalized nearest-neighbor hopping parameter t_0. As the angle θ is increased away from the nodal direction, the energies $E_{\boldsymbol{k}}^{+}$ and $E_{\boldsymbol{k}}^{-}$ no longer meet but split and there is a clear gap between them. Both move down in energy but not by the same amount. Also, the maximum and minimum corresponding to a given pair of curves do not fall at exactly the same value of

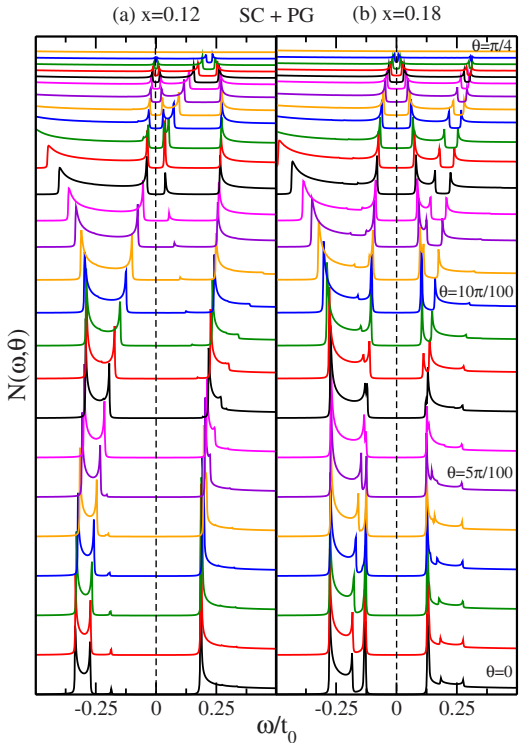

FIG. 7. (Color online) The partial DOS $N(\omega,\theta)$ as a function of ω in units of t_0 for two values of doping (a) $x=0.12$ and (b) $x=0.18$. From top to bottom, the curves are shown from $\theta=\pi/4$ to $\theta=0$ in steps of $\pi/100$.

k. In the above sense, the two van Hove singularities at issue which define the pseudogap peaks in $N(\theta,\omega)$ of Fig. 7 are not entirely symmetric. The energies of the Dirac point can easily be traced as a function of doping. It corresponds to the point $E_{\boldsymbol{k}}^{+}=E_{\boldsymbol{k}}^{-}$ which occurs for $\xi_{\boldsymbol{k}}+\xi_{\boldsymbol{k}}^{0}=0$, i.e., $E_{\boldsymbol{k}}=\sqrt{\tilde{\xi}_{\boldsymbol{k}}^2+\Delta_{\mathrm{pg}}^2(\boldsymbol{k})}=0$ for $\theta=\pi/4$, and the details of the disper-

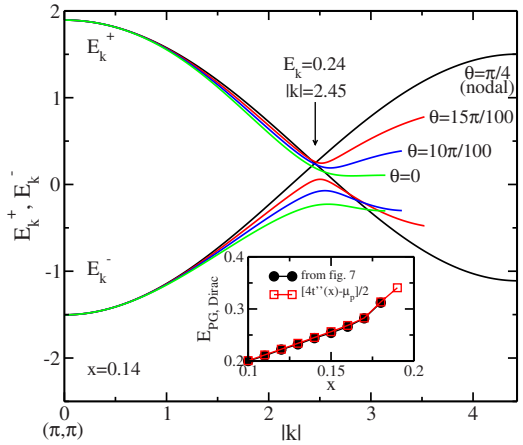

FIG. 8. (Color online) The variation in the energies $E_{\boldsymbol{k}}^{+}$ and $E_{\boldsymbol{k}}^{-}$ with magnitude of momentum $k=|\boldsymbol{k}|$, measured from (π,π), for various fixed values of the angle θ defined in Fig. 1 as indicated in the figure. The inset gives the energy of the pseudogap Dirac point as a function of doping x. Results for our complete numerical calculations from curves as shown in Fig. 7 are compared with the approximate formula $E_{\mathrm{dirac}}=(4t''-\mu_p)/2$.

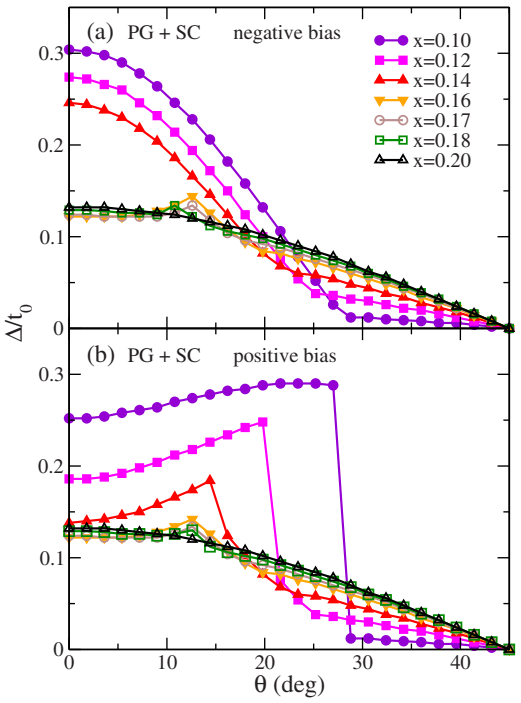

FIG. 9. (Color online) The energy gap read off the curves for $N(\omega,\theta)$ of the type shown in Fig. 7 as a function of θ in the Brillouin zone measured from (π,π). The top frame is for negative bias (occupied states) and the bottom for positive bias (unoccupied states). Note the isotropy between these two sets of data for angles around 45° or $\pi/4$ (nodal direction) and the large anisotropy at small angles (antinodal).

sion curves determine the critical value of $k \equiv k_c$. For $x=0.14$, this $k_c=2.45$ in Fig. 8 which is somewhat larger than the value $\pi/\sqrt{2}$ which corresponds to $k_x=k_y=\pi/2$. For this latter point, the dispersion curves of YRZ are particularly simple and only third neighbor hopping survives. Taking $E_{\boldsymbol{k}}=0$ but using $k_x=k_y=\pi/2$ to evaluate the remaining expression, provides an approximate estimate for the energy of the Dirac point E_{dirac} as $[4t''(x)-\mu_p]/2$. This estimate is shown in the inset of Fig. 8 to be quite adequate and shows how E_{dirac} moves toward zero energy as x decreases, as is also seen in Fig. 7 where the pseudogap Dirac point is seen as the closing of the pseudogap coherence peaks at $\theta=\pi/4$.

Returning now to this Fig. 7, we note that as θ is decreased toward the antinodal direction, it remains possible to identify unambiguously a lowest energy peak and the magnitude of the energy at which these peaks occur is recorded in Fig. 9 as a gap in units of t_0 for each angle. For optimum or even near optimum doping, the resulting curve is close to a simple $\cos(2\theta)$ curve and represents the superconducting gap. However, it should be noted that the curves for $x=0.18$, 0.17, and 0.16 all show an additional structure between 10° and 15° and the overall curve does deviate visibly from a simple $\cos(2\theta)$. This is not surprising since near $x \lesssim 0.2$, the Fermi surface, as we have shown in Fig. 1, has reconstructed from the large open surface of FLT to Luttinger surfaces (holes about the nodal region and electrons about the antinodal point) and the partial DOS $N(\omega,\theta)$ has some knowledge of this fact. Consequently, the extracted energy scale is not a pure superconducting gap scale. Nevertheless, the distortions from a pure $\cos(2\theta)$ are not large and the curves show almost perfect particle-hole symmetry (compare the top and bottom frame of Fig. 9 for $x \geq 0.16$).

The situation is quite different and more interesting for low dopings approaching closer to the Mott transition. In that case, only a Luttinger hole pocket remains as shown in Fig. 1. When superconductivity is not considered, there are zero energy excitations along the Luttinger contours which are real Fermi surfaces and these are gapped by superconductivity. But for angles smaller than θ_h, no true Fermi surface exists and consequently, the peaks seen in $N(\omega,\theta)$ [Fig. 7(a)] no longer have their origin in $\Delta_{\text{sc}}(\boldsymbol{k})$ but are related rather to the pseudogap $\Delta_{\text{pg}}(\boldsymbol{k})$. This can be easily traced in Fig. 7(a) for $x=0.12$. In the nodal direction, the peaks nearest $\omega=0$ are the superconducting coherence peaks and these become more prominent as the gap opens up. But eventually, particularly on the positive bias side, they start to lose intensity while at the same time, the pseudogap peak at higher energy remains quite intense and it is this peak that must eventually be taken if we are to characterize $N(\omega,\theta)$ for smaller values of θ with a single energy scale as we are doing here. It is clear that we need to jump from one energy scale to the other. On the negative bias side, however, the progression with decreasing θ remains smooth. We always take the large intensity peak closest to the origin $\omega=0$. These facts are reflected in Fig. 9. In the top frame for $x \leq 0.14$, we see two very distinct gap scales: a superconducting one for θ near 45° and a pseudogap one for θ going toward zero. The curves have a kink at an angle corresponding to $\theta=\theta_h$, the end of the Luttinger pocket, but otherwise they show a rather smooth behavior. On the other hand, for positive biases (lower frame of Fig. 9) there is a clear jump in the curves as we transfer from superconducting to pseudogap scale and this is followed by a progressive drop to lower values as θ decreases toward zero in sharp contrast to the top frame for negative ω.

To make clearer that our results for the frequency dependence of $N(\omega,\theta)$ cannot be fit by the simple formula of Eq. (9), we have used this formula along with the gaps presented in Fig. 9 to recalculate a total DOS $N(\omega)$ according to Eq. (8) with weights $W(\theta)$ set equal to one for simplicity. Numerical results are presented in Fig. 10(b). For ease of comparison, we have reproduced in Fig. 10(a) the full DOS already presented in Fig. 3 on which our angular decomposition is based. For small values of ω, we see a great deal of agreement between these two sets of figures. Near optimum doping only the superconducting gap scale is prominent while for the highly underdoped regime both superconducting and pseudogap scales are clearly seen. At larger energies important differences arise and these have their origin in the failure of Eq. (9) with a single energy scale to capture all the details present in the partial densities of states of Fig. 7. In particular, the van Hove singularity seen on the negative bias side in the top frame is completely missed in the lower frame. While this figure speaks to the limitation in the method used to extract energy gaps from STS data[28] it also shows that important qualitative and even semiquantitative information can be extracted in this way. Some details are certainly missed but other important features are quite prominently seen such as the pseudogap scale and its asymmetry. One

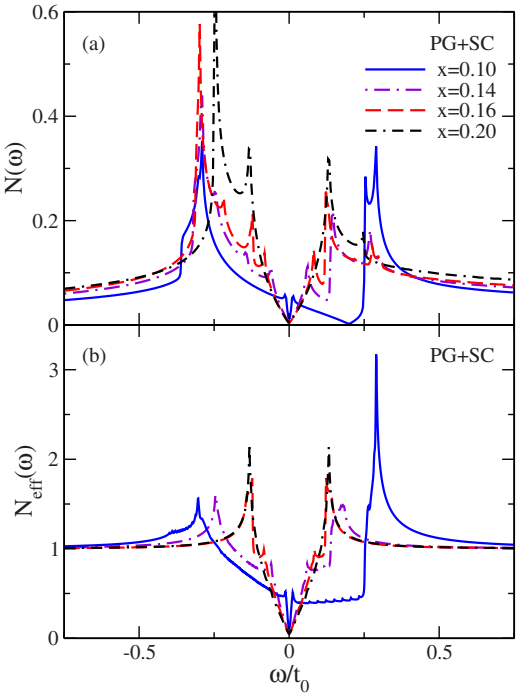

FIG. 10. (Color online) Comparison of (a) the original DOS $N(\omega)$ from Fig. 3 with (b) the quasiparticle DOS $N_{\text{eff}}(\omega)$ versus ω in units of t_0 as defined by Eqs. (8) and (9). Both (a) and (b) refer to the state with superconductivity and the pseudogap present.

could improve the agreement between the top and bottom frames in Fig. 10 by including weights $W(\theta)$ or multiplying $N_{\text{eff}}(\omega)$ by an envelope function, which partially accounts for the presence of the van Hove singularity present in our model band structure but this is not our aim here.

In Fig. 11, we provide a direct comparison between our results for the asymmetry between positive and negative biases of the derived angular dependent gap and the data of Pushp *et al.*[28] for the same quantity. Plotted is the ratio of $\Delta_{-\text{bias}}/\Delta_{+\text{bias}}$ from our Fig. 9 for $x=0.12$ (squares) and 0.14

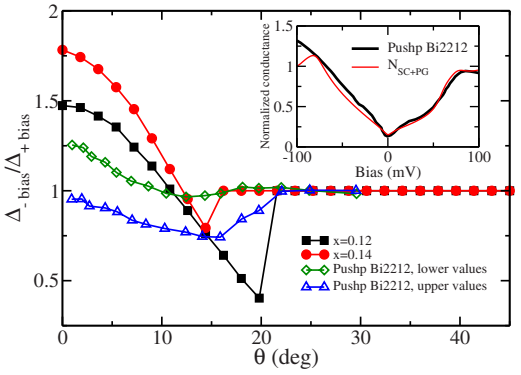

FIG. 11. (Color online) The ratio of $\Delta_{-\text{bias}}/\Delta_{+\text{bias}}$ versus angle, taken from Fig. 9 for $x=0.12$ and 0.14. The theoretical work is compared with the data of Pushp *et al.* (Ref. 28) which is bounded by the diamonds and triangles (see text for details). Inset: a comparison between the theory and experiment for the normalized conductance (thick black curve) of Pushp *et al.* and a DOS curve from our calculations (thin red curve).

(circles). Pushp *et al.*[28] show several curves in Fig. S3 for a range of data taken from several spots on their UD58 sample. As the negative bias data are fairly uniform, we took points from along the trend of the data. For the positive bias, there is a range of values for each angle and so we took the highest and lowest values to form separately the ratio with the negative bias data. This is shown as the blue triangles and green diamonds, respectively. As we wish to concentrate on the asymmetry, only the data for angles less than 30° are shown. Due to the expected symmetry for angles in the nodal region, the data ratio toward the nodal region have been normalized to one to facilitate comparison with theory even though the ratio in the data was slightly greater than one. Our procedure is not entirely rigorous and in the hands of the experimentalists there might be a more accurate analysis of the result. Nevertheless, while the individual curves for Δ_+ and Δ_- are quite different in shape as compared with our theoretical results, we find that the ratio shows the same qualitative trend as theory. There is a significant dip around $15°-20°$ followed by a rise as the antinodal region is approached. This comparison provides evidence that the pseudogap forms asymmetrically about the Fermi surface as in our model. In the inset of Fig. 11, we show results for the DOS in the resonating valence bond spin liquid compared with UD35 data from Pushp *et al.*[28] (Fig. S4). We used $x=0.11$ to match the T_c reduction from optimum and have added broadening and a linear incoherent background to provide a better fit to the data. This linear background does not alter the structures due to the two energy gaps in the model. The agreement is good in the low-energy region shown and it again clearly reveals asymmetry between positive and negative biases.

V. ZERO FREQUENCY LIMIT

We finally turn to the slope of the DOS at $\omega \to 0$ shown in Fig. 12(a). In YRZ theory, the superconducting Dirac point [shown schematically by Fig. 12(b)], on the heavily weighted side of the Luttinger hole pocket in the nodal direction, is not affected by pseudogap formation. For small energies ω, it is clear from the cone shown in Fig. 12 that the only excited states available are those near the bottom tip of the Dirac cone. We can easily show that, as for an ordinary FL,[29] the slope is given by

$$s = \frac{g_t}{\pi v_\Delta v_F} \tag{11}$$

with $N(\omega)=s|\omega|$. Here, v_F is the Fermi velocity at the Dirac point and $v_\Delta=|\nabla\Delta_{\text{sc}}(k)|_{k_F}=(\Delta_{\text{sc}}^0/\sqrt{2})|\sin(k_{Fx})|$ is the superconducting gap velocity at this same point. In the inset of Fig. 12(a), we show results of complete numerical calculations of the DOS for the case of $x=0.14$ with both pseudogap and superconducting gap included (solid black curve) and compare with the results of Eq. (11) (dashed red line). We see good correspondence.

Formula (11) is the same as would hold in a FL with two very important differences: g_t and a possible variation in v_Δ in this model. In Eq. (11), the Gutzwiller coherence factor $g_t(x)$ carries the information on how much weight remains in

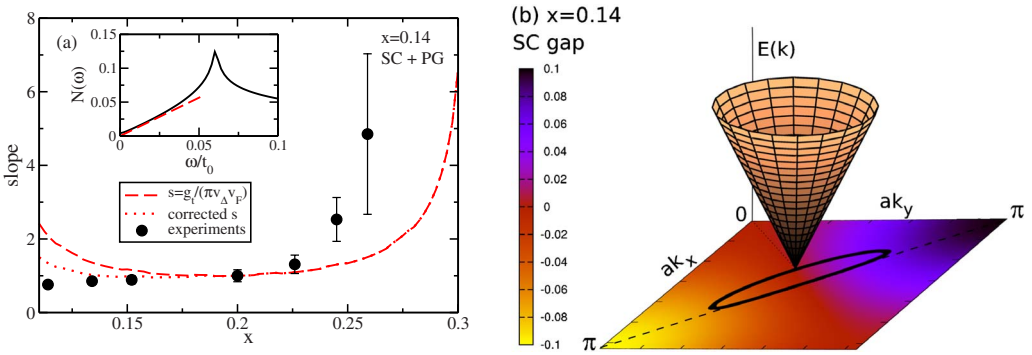

FIG. 12. (Color online) (a) The slope of $N(\omega)$ normalized to that for optimal doping versus x compared with the data from Pushp *et al.* (Ref. 28). Inset: $N(\omega)$ for $x=0.14$ with both the superconducting gap and pseudogap present showing the linear behavior at low ω in agreement with Eq. (11) which is shown as the red dashed line. (b) A schematic of the superconducting Dirac cone as it grows in energy out of the nodal region on the heavily weighted side of the Luttinger hole pocket. The heavy solid black curve is the Luttinger contour for $x=0.14$.

the coherent part of the Green's function when correlation effects are included, with the rest shifted to incoherent processes. This factor is a crucial part of our present approach but does not enter FLT. An important consequence of this fact is that it reduces the rise in the slope in the highly underdoped regime of the cuprate phase diagram as compared with a pure FL approach. It provides a factor of $2x/(1+x)$ while the gap velocity is proportional to T_c. Pushp *et al.*[28] found in STS data that the slope was nearly constant over a significant doping range below optimum. Matching their reduction from optimum of the T_c of their samples with our superconducting dome in order to determine the relation to the doping x used in our model, we plot the slope of their data normalized to the value at optimum versus x. As there was a range of values in their data for a particular doping, we have done our best to indicate this as a point with a bracketing bar. Comparison with this data (solid black circles in Fig. 12) shows that, around $x \simeq 0.10$ which is the doping in our calculations that corresponds to a reduction in T_c by a factor of 3 below its value at optimum, the predicted slope represented by the dashed red curve starts to increase while experiment does not. This could mean that in reality the Gutzwiller factor is a more strongly decaying function of x than the one we have used. Alternatively, broadening will have the tendency to decrease the slope. However, so far we are neglecting another important effect associated with the YRZ model. In this model the gap to T_c ratio $2\Delta_{sc}^0/k_B T_c$, which for simplicity we have fixed at a value of 6 in all our calculations, is known to vary importantly with x. In very recent work, Schachinger and Carbotte[30] have solved a generalized BCS gap equation with the pseudogap and Fermi-surface reconstruction fully accounted for and have found that this ratio changes from its canonical value of 4.3 at $x=0.2$ (optimum) to ~ 6.5 or even higher toward the end of the dome as the Mott insulator and antiferromagnetism is approached. Accounting for this reduces the variation in slope between optimum and highly underdoped by $\sim 50\%$, bringing our calculations much closer to experiment as indicated by the red dotted curve in Fig. 12(a). The overall agreement between theory and the data is very good. It is important to stress that $g_t(x)$ provides an important factor in Eq. (11) which brings theory much closer to experiment than what one would find in a FL approach and this also is true as well for the variation in gap to critical temperature ratio.

VI. SUMMARY AND CONCLUSIONS

We have computed the total quasiparticle DOS in the resonating valence bond spin liquid model[1] of the underdoped cuprates. When superconductivity is not included, the formation of the pseudogap, which provides a mechanism for Fermi-surface reconstruction, modifies the underlying Fermi-liquid DOS in an asymmetric way with respect to the Fermi energy ($\omega=0$). For small values of the pseudogap just below the critical doping associated with a QCP, the resulting depression in $N(\omega)$ is confined to negative energies. As doping is reduced toward the Mott insulating state, the depression deepens, covers a larger range in energy and spans positive as well as negative biases but its effect remains asymmetric. However, if superconductivity is also included, particle-hole symmetry is restored at lower energies of order $\Delta_{sc}^0(x)$, although beyond this range the asymmetry associated with the pseudogap remains. This effect is traced to the fact that the pseudogap is associated with the antiferromagnetic Brillouin zone rather than the Fermi surface where the superconducting gap opens.

One can trace peaks in the total quasiparticle DOS which are, at optimum doping and just below, coherence peaks due to superconductivity but these evolve for $x \lesssim 0.16$ into pseudogap peaks which are distinctly different for positive and negative biases. This asymmetry is an intrinsic part of the YRZ model and can be used to test its validity. We are also able to trace a second set of peaks associated with the superconducting gap which however originate from the end of the Luttinger hole pocket at an angle θ_h in the Brillouin zone. In the heavily underdoped region of the phase diagram, these peaks are the only ones that can be identified as due purely to the superconducting gap. These signatures are relatively weak, however, as found in, for example, the experiments of Boyer *et al.*,[31] in comparison with those seen in an ordinary d-wave BCS superconductor. As a function of doping, the energy corresponding to these coherence structures

follow the dome associated with the critical temperature although the scale of the effective gap involved is reduced.

When the total DOS is decomposed into partial contributions from each angle θ in the Brillouin zone separately, $N(\omega,\theta)$, it is found that at some angles $N(\omega,\theta)$ can show complex behavior as a function of energy ω and even display several peaks. Such distributions cannot be modeled by the simple function of Eq. (9). Nonetheless, we find that we could identify, in a fairly unambiguous fashion, a single peak in these distributions which was both close to the origin $\omega=0$ and had significant amplitude. This provides a single energy scale for each direction θ. At angles near the nodal direction, this scale is associated with the superconducting gap but as θ is decreased it progresses into a peak associated with the pseudogap energy. In some cases the transition from one scale to the other is smooth while in others it can be abrupt and also somewhat ambiguous. What is found is that the superconducting gap peak at low energies rapidly loses intensity while the pseudogap peak at higher energies is quite intense and so dominates over the lower energy structure and thus must be chosen as characteristic of a single gap scale for this angle θ in the Brillouin zone. This gap can however differ considerably in size depending on the sign of the bias involved. For energy below the superconducting gap scale, there is little asymmetry but this changes radically as the antinodal direction is approached in the highly underdoped regime where the pseudogap is probed. Our findings have implications for the analysis of STS data when one wishes to extract directional information from such experiments.[28] Comparison with the data of Pushp *et al.* for both $N(\omega)$ and $\Delta_{-\mathrm{bias}}(\theta)/\Delta_{+\mathrm{bias}}(\theta)$ shows indeed an asymmetry in the DOS which is in qualitative agreement with the YRZ model.

Another result is that the zero energy slope of the DOS is importantly reduced from its FL value in YRZ theory because of the appearance of a Gutzwiller factor $g_t(x)$ which is a rapidly decreasing function as x decreases and represents the reduction, due to correlation effects, of the coherent part of the charge-carrier Green's function. This factor can partially compensate for the rapid increase in slope that would occur due to the appearance of the gap velocity v_Δ in the denominator of the expression for the slope in ordinary BCS theory. However, this factor is modulated by a rapid increase in the value of gap to critical temperature found to be the direct consequence of an increase in the pseudogap in the theoretical work of Schachinger and Carbotte.[30] Without these two effects there would be a serious conflict between theory and the experimental results of Pushp *et al.*[28] who find a slope which remains fairly constant in the underdoped regime. While a comparison with the existing data and YRZ predictions gives qualitative agreement, there are indications that the Gutzwiller factor $g_t(x)$ and/or the gap to T_c ratio may in fact vary more rapidly with decreasing x than indicated by theory.

ACKNOWLEDGMENTS

We thank James LeBlanc for his assistance and helpful discussions. This work has been supported by NSERC of Canada and by the Canadian Institute for Advanced Research (CIFAR).

*enicol@uoguelph.ca

[1] K.-Y. Yang, T. M. Rice, and F. C. Zhang, Phys. Rev. B **73**, 174501 (2006).
[2] V. J. Emery and S. A. Kivelson, Nature (London) **374**, 434 (1995).
[3] S. Chakravarty, R. B. Laughlin, D. K. Morr, and C. Nayak, Phys. Rev. B **63**, 094503 (2001).
[4] J.-X. Zhu, W. Kim, C. S. Ting, and J. P. Carbotte, Phys. Rev. Lett. **87**, 197001 (2001).
[5] B. Valenzuela and E. Bascones, Phys. Rev. Lett. **98**, 227002 (2007).
[6] J. P. F. LeBlanc, J. P. Carbotte, and E. J. Nicol, Phys. Rev. B **81**, 064504 (2010).
[7] J. P. F. LeBlanc, E. J. Nicol, and J. P. Carbotte, Phys. Rev. B **80**, 060505(R) (2009).
[8] E. Illes, E. J. Nicol, and J. P. Carbotte, Phys. Rev. B **79**, 100505(R) (2009).
[9] K.-Y. Yang, H. B. Yang, P. D. Johnson, T. M. Rice, and F. C. Zhang, EPL **86**, 37002 (2009).
[10] E. Bascones and B. Valenzuela, Phys. Rev. B **77**, 024527 (2008).
[11] K. Yang, K. Huang, W. Chen, T. Rice, and F. Zhang, arXiv:1005.3441 (unpublished).
[12] J. P. Carbotte, K. A. G. Fisher, J. P. F. LeBlanc, and E. J. Nicol, Phys. Rev. B **81**, 014522 (2010).
[13] E. J. Nicol and J. P. Carbotte, Phys. Rev. B **44**, 7741 (1991).
[14] E. Schachinger, J. P. Carbotte, and F. Marsiglio, Phys. Rev. B **56**, 2738 (1997).
[15] E. Schachinger and J. P. Carbotte, Phys. Rev. B **62**, 9054 (2000).
[16] E. Schachinger, J. J. Tu, and J. P. Carbotte, Phys. Rev. B **67**, 214508 (2003).
[17] J. P. Carbotte, E. Schachinger, and J. Hwang, Phys. Rev. B **71**, 054506 (2005).
[18] F. Marsiglio, J. P. Carbotte, A. Puchkov, and T. Timusk, Phys. Rev. B **53**, 9433 (1996).
[19] E. J. Nicol, J. P. Carbotte, and T. Timusk, Phys. Rev. B **43**, 473 (1991).
[20] J. P. Carbotte, C. Jiang, D. N. Basov, and T. Timusk, Phys. Rev. B **51**, 11798 (1995).
[21] H. K. Leung, J. P. Carbotte, D. W. Taylor, and C. R. Leavens, Can. J. Phys. **54**, 1585 (1976).
[22] C. O'Donovan and J. P. Carbotte, Phys. Rev. B **52**, 4568 (1995).
[23] C. O'Donovan and J. P. Carbotte, Physica C **252**, 87 (1995).
[24] F. Marsiglio, R. Akis, and J. P. Carbotte, Phys. Rev. B **36**, 5245 (1987).
[25] B. Mitrović, C. R. Leavens, and J. P. Carbotte, Phys. Rev. B **21**, 5048 (1980).
[26] E. Schachinger, J. M. Daams, and J. P. Carbotte, Phys. Rev. B **22**, 3194 (1980).
[27] M. Le Tacon, A. Sacuto, A. Georges, G. Kotliar, Y. Gallais, D. Colson, and A. Forget, Nat. Phys. **2**, 537 (2006).

[28] A. Pushp, C. V. Parker, A. N. Pasupathy, K. K. Gomes, S. Ono, J. Wen, Z. Xu, G. Gu, and A. Yazdani, Science **324**, 1689 (2009).
[29] A. C. Durst and P. A. Lee, Phys. Rev. B **62**, 1270 (2000).
[30] E. Schachinger and J. P. Carbotte, Phys. Rev. B **81**, 014519 (2010).
[31] M. C. Boyer, W. D. Wise, K. Chatterjee, M. Yi, T. Kondo, T. Takeuchi, H. Ikuta, and E. W. Hudson, Nat. Phys. **3**, 802 (2007).